Ruthenium Triazine Composite: A Good Match for Increasing Hydrogen Evolution Activity through Contact Electrification

Qiangjian Ju, Ruguang Ma, Yu Pei, Beibei Guo, Zichuang Li, Qian Liu, Tiju Thomas, Minghui Yang,* Graham J. Hutchings, and Jiacheng Wang**

Q. Ju, Dr. R. Ma, Dr. Y. Pei, B. Guo, Z. Li, Prof. Q. Liu, Prof. J. Wang
The State Key Laboratory of High Performance Ceramics and Superfine Microstructure, Shanghai Institute of Ceramics, Chinese Academy of Sciences, 1295 Dingxi Road, Shanghai 200050, China
Email: maruguang@mail.sic.ac.cn; jiacheng.wang@mail.sic.ac.cn

Q. Ju, Dr. R. Ma, Prof. M. Yang, Prof. J. Wang
Center of Materials Science and Optoelectronics Engineering, University of Chinese Academy of Sciences, Beijing 100049, China

Prof. G. Hutchings
Cardiff Catalysis Institute, School of Chemistry, Cardiff University, Main Building, Park Place, Cardiff, CF10 3AT, U.K.

Q. Ju, Prof. M. Yang
Ningbo Institute of Materials Technology and Engineering, Chinese Academy of Sciences, 1219 Zhongguan West Road, Ningbo 315201, China
Email: myang@nimte.ac.cn

Dr. T. Thomas
Department of Metallurgical and Materials Engineering, Indian Institute of Technology Madras, Adyar, Chennai 600036, Tamil Nadu, India

Q. Ju
University of Chinese Academy of Sciences, 19A Yuquan Road, Shijingshan District, Beijing 100049, China

Keywords: electrocatalysis, nanocomposite, electron acceptor, contact electrification, theoretical calculation

Abstract: The development of Pt-free catalysts for the alkaline hydrogen evolution reaction (HER), which is widely used in the industrial scale water-alkali electrolyzers, remains a contemporary and pressing challenge. Ruthenium (Ru) has excellent water-dissociation ability and could be an alternative water splitting catalyst. However, its large hydrogen binding energy limits the HER activity. Here, a new approach has been proposed to boost the HER activity of Ru through uniform loading of Ru nanoparticles on triazine-ring (C3N3)-doped carbon (triNC). The composite (Ru/triNC) exhibits outstanding HER activity with an ultra-low overpotential of ~2 mV at 10 mA cm^{-2}; thereby making it the best performing electrocatalyst hitherto reported

for alkaline HER. The calculated metal mass activity of Ru/triNC is >10 and 15 times higher than that of Pt/C and Pt/triNC. Both theoretical and experimental studies reveal that triazine-ring is a good match for Ru to weaken the hydrogen binding on Ru through interfacial charge transfer via increased contact electrification. Therefore, Ru/triNC can provide the optimal hydrogen adsorption free energy (approaching zero), while maintaining the strong water-dissociation ability. This study provides a new avenue for designing highly efficient and stable electrocatalysts for water splitting.

1. Introduction

Hydrogen is a clean and green energy source. Despite existing challenges (e.g. viable and scalable hydrogen storage options), hydrogen production is a key activity in the movement towards a renewable and clean energy based economy.[1] Electrochemical water splitting is an eco-friendly way to produce hydrogen with no emission of pollutants. This is in stark contrast to the significantly polluting options currently used in industry (e.g. steam reforming of methane or coal to obtain hydrogen). Generally, the hydrogen evolution reaction (HER) is straightforward and efficient in acidic media due to the availability of H^+ (see details in Supporting Information). However, in industrial situations, alkaline media for water splitting/hydrolysis is preferred; this is because it accelerates the oxygen evolution kinetics.[2] Pt/C is the state-of-the-art HER electrocatalyst in acidic solution. However, its activity and stability significantly decrease in alkaline conditions. Thus, an alternative alkaline HER catalyst is a contemporary requirement.

The adsorption characteristics of the reaction intermediates ($*H$, in this case) is an important factor in determining the HER activity of electrocatalysts.[3-5] Moderate adsorption enthalpy of $*H$ ($\Delta G_H \approx 0$) is considered desirable.[3, 6] Weak hydrogen binding ($\Delta G_H > 0$) leads to the difficulty in the Volmer step, while strong adsorption ($\Delta G_H < 0$) is not beneficial to the desorption of products in the Tafel or Heyrovsky steps. Also, water dissociation ($H_2O+e^-+* \rightarrow *H+OH^-$) is the primary concern in alkaline HER.[7] Notably, some (hydro)oxides and oxides such as $Ni(OH)_2$[8] and CrO_x[9] demonstrate the ability to reduce the water dissociation barriers in alkaline conditions when used as co-catalysts. Some metals with strong water-dissociation ability, such as Raney (or spongy) Ni and Ni alloys,[10] are efficient alkaline HER catalysts. However, these alloys are usually not sufficiently active when compared to noble metals such as Pt.

Previous reports suggest that the energy barrier for water dissociation is low on Ru surfaces due to the strong interaction with the oxygen atoms of water molecules.[11] This has been consistently known from both computation and experiment.[12] This makes Ru a viable candidate for alkaline HER catalysis. However, it is found that Ru has a rather strong hydrogen adsorption ability, which leads to difficulty in the Tafel step.[13, 14] Through rational materials design,[12, 15] control of the support,[14, 16-18] and electronic structure modification,[19] Ru could in fact show HER activities similar to Pt, or even better. However, despite this possibility, elucidation of principles for improving the HER activity of Ru has remained elusive. It has been reported that the Ru surface is an 'electron donor' substrate for hydrogen binding.[20] Hence, identification of a support which can increase electron transfer from Ru to the support could

help. This is because doing so will effectively weaken hydrogen binding on Ru, thus resulting in an improved HER performance.

Contact electrification[21, 22] at the metal-conductor/semiconductor interface, is associated with electron transfer that occurs when the two components are in contact. This is caused by differences in the Fermi levels and work functions of the components that are in contact with each other. Electrons transfer across the junction of the components to equalize the Fermi levels. This phenomenon offers a reasonable means to influence the electron transfer process occurring in HER.[21, 23] By choosing appropriate conductive supports, the electron transfer processes could thus be controlled.

Here, we design and demonstrate a unique carbon support doped with N-rich triazine-ring (C_3N_3) that can act as an active "electron acceptor" when contacting Ru.[24, 25] Ru on this triazine-ring-doped carbon (Ru/triNC) exhibits the outstanding HER activity when compared to commercial Pt/C in alkaline solution. In fact, based on champion HER catalysts reported thus far, it is evident that Ru/triNC is the best-performing electrocatalyst.[14, 17, 18, 26] We report the relationship between the HER activity of the supported Ru nanoparticles and work functions of the different carbon supports (pure carbon (C), N-doped carbon (NC), and triNC). It is found that the catalytic performance of Ru is significantly influenced by contact electrification with the carbon substrates. Compared to C and NC, triNC promotes more electron loss from Ru and hence weakens hydrogen binding.

2. Results and discussion

2.1. Synthesis and characterization of Ru/triNC

The steps used to synthesize the triazine-based covalent triazine framework (CTF), triazine-ring doped carbon (triNC) and triNC-supported Ru (Ru/triNC) are shown in Scheme 1. Briefly, CTF and triNC are fabricated using an ionothermal strategy with tetracyanoquinodimethane (TCNQ) as the raw material.[24, 25] Ru is loaded on triNC using an impregnation step followed by a thermal reduction process (details are given in Electronic Supplementary Material). To study the differences among several types of (i) carbon supports and (ii) levels of nitrogen doping, Ketjen black (C) and N-doped Ketjen black (NC) are chosen to support Ru nanoparticles. This is done due to their high electrical conductivity and large specific surface area (SSA, ~1300 $m^2 g^{-1}$). Ru is also supported on C and NC using the same process as the preparation of Ru/triNC. The resulting samples are denoted as Ru/C and Ru/NC, respectively.

To confirm the existence of the triazine-ring structure, Fourier-Transform Infrared (FT-IR) spectroscopy is conducted for the triazine-based CTF and triNC based samples (Figure 1a). The adsorption peak at ~2200 cm^{-1} corresponds to -C≡N stretching vibration.[24] This peak disappears after pyrolysis, indicating the -C≡N decomposition. The adsorption peaks at ~1560 cm^{-1} and ~1180 cm^{-1} are attributed to the vibration of triazine and benzene,[24] indicating the formation of triazine-ring within the carbon matrix. Two peaks of triazine ring are reserved even after further annealing, confirming the existence of triazine ring in triNC. Except for TCNQ, we have tried other raw materials (e.g. 1,4-dicyanobenzene) for CTF, but these CTF materials would not tolerate the further pyrolysis and decomposed at higher pyrolysis temperature. This indicates that CTF made from TCNQ shows better thermal stability which still remains after annealing at higher temperature. The specific surface area of triNC is evaluated using nitrogen adsorption measurements at -196 °C (Figure S1). The sorption isotherms belong to the reversible adsorption profiles of mixed type I and type IV. The isotherm concave to P/P_0 axis and adsorption amount approach a limit as P/P_0 is close to 1, also an obvious hysteresis loop appear in the high relative pressure range. This indicates the coexistence of microporous and mesoporous structure in triNC. The calculated specific surface area (SSA) of triNC using Brunauer-Emmett-Teller (BET) is as high as ~2000 $m^2 g^{-1}$. The corresponding

pore size distribution analyzed by nonlocal density function theory (NLDFT) also shows a micro-mesoporous structure. The ultrahigh SSA and an abundance of micropores originate from the 3D amorphous framework of CTF. The X-ray diffraction (XRD) pattern of triNC shows two broad reflections at ~25° and ~45°, consistent with its amorphous structure (Figure 1b). The reflections associated with the hexagonal Ru appear for Ru/triNC, clearly confirming the presence of Ru.

The morphology of the samples prepared is observed using TEM (Figure 1c-f and Figure S2-4). High resolution TEM (HRTEM) micrograph shows that triNC has an amorphous structure (Figure S2). SEM and low-resolution TEM images show no aggregation of Ru in Ru/triNC prepared at 900 °C (Figure S3-4). Ru nanoparticles are well-dispersed within the triNC matrix, and their particle sizes are typically in the range of ~4-7 nm (inset of Figure 1c). The average size of over 200 nanoparticles that we counted is 5.7 nm. The high-angle annular dark-field scanning TEM (HAADF-STEM) image confirms the formation of small-sized nanoparticles, revealing lots of bright spots (Figure 1d). From the HRTEM image of Ru/triNC (Figure 1e), it is clear that Ru nanoparticles are crystalline with a lattice spacing of ~2.13 Å; this corresponds to the (002) plane of hexagonal Ru.[16] The lattice of carbon (~3.55 Å) is also visible around Ru particles. This shows that the addition of Ru metal promotes the graphitization of carbon supports.[27] Elemental mapping images demonstrate that N elements are distributed around Ru nanoparticles, implying rather uniform distribution of Ru on the triazine-ring (Figure 1f). Ru nanoparticles in Ru/C and Ru/NC (Figure S4) have similar particle sizes when compared to those in Ru/triNC. XRD also reveals the presence of hexagonal Ru for Ru/C and Ru/NC, as is the case for Ru/triNC (Figure S5). The real loading amounts of Ru in all Ru/triNC samples are determined by thermogravimetric analysis (TGA) in air atmosphere. The obtained TG curves are shown in Figure S6. During the test, the carbon support can be oxidized into CO_2 and Ru could transform into RuO_2. The calculated Ru contents are 2.3 wt% for Ru/triNC1, 5.8 wt% for Ru/triNC5, 9.4 wt% for Ru/triNC and 14.8 wt% for Ru/triNC20, respectively. These Ru contents match well with the expected.

2.2. Contact electrification of Ru and supports

Contact electrification and electron transfer for different samples are studied *via* ultra-violet photoelectron spectroscopy (UPS) and X-ray photoelectron spectroscopy (XPS). UPS is conducted to measure work functions of different carbon supports before and after adding Ru. In the UPS spectra (Figure 2a-b), E_{Fermi} is located at 0 eV and the work functions for the materials can be determined from the shift of the secondary electron cut-off edge. As expected, pure C has the most positive $E_{cut\text{-}off}$ (~16.7 eV) and this $E_{cut\text{-}off}$ shifts negatively by ~0.2 eV for NC. This indicates that doping using hetero-elements with higher electronegativity increases the work function of carbon.[28] The triNC shows the most negative $E_{cut\text{-}off}$ located at ~16.1 eV, implying that it has the lowest Fermi level among these three samples. The change of Fermi level and work function mainly originates from the local nitrogen concentration of triazine-ring. Hence, compared to C and NC, triNC has the strongest electron acceptance ability during the contact electrification with Ru. Figure 2b and Figure S7 show the change in work function of different carbon supports before and after addition of Ru. It is evident that, after the addition of Ru, the cut off edge of carbon supports shifts positively, due to two main reasons. Firstly, Ru nanoparticles with lower work function contribute to the secondary electrons that have higher kinetic energies.[29] Secondly, since UPS reflects the valence electron character of whole surface, charge transfer from Ru to carbon support makes the material surface electron-rich. These results further show the charge redistribution after the addition of Ru.[21]

The electron transfer process and valence states of Ru supported on different carbon supports are further confirmed using XPS. In the N1s spectra of triNC and Ru/triNC (Figure 2c), nitrogen possesses two peaks which are ascribed to triazine-ring N (398.8 eV) and graphitic

N (400.2 eV), respectively. Graphitic N originates from the separation of the triazine-ring during carbonization. By comparing the areas of two peaks, we determine that the triazine-ring groups remain even after thermal treatment (Figure S9 and Table S1). The N1s spectra show a similar but wide peak after the addition of Ru, reflecting the occurrence of electron redistribution between Ru and triNC. The peak of the triazine-ring N shows a negative shift of ~0.2 eV, while the peak of graphitic N does not change. This reveals that the triazine-ring with a higher local nitrogen density is the main electron capturing site. The Ru 3p spectra exhibits double peaks at ~462.4 and ~484.8 eV (Figure 2d), which correspond to zero-valence $Ru3p_{1/2}$ and $3p_{3/2}$, respectively. When compared to Ru/C, the binding energies of Ru 3p in Ru/NC negatively shift by~0.4 eV, suggesting that electron transfer occurs from Ru to NC. Ru/triNC reveals the most positive shift among three samples, indicating the highest electron loss occurs in case of Ru loaded onto triNC. The conspicuous positive shifts for Ru/C, Ru/NC and Ru/triNC are consistent with the UPS analysis above.

The electron transfer occurring between Ru and triNC is further captured using First-principle calculations. First of all, the work functions of C, NC and triNC are calculated (Figure 3a and Table S2). The calculated work functions match well with the experimental results. It clearly indicates that the Fermi level is influenced by N doping and moves to the deeper energy levels.[28] The charge transfer process is analyzed using differential charge density (Figure 3b). To simplify the calculations, we simulate a graphene structure with a triazine-ring defect and put a 6-atom Ru cluster on it to mimic Ru/triNC. The structure (after relaxation) is given in Figure 3b (left panel). The distortion of triazine ring on graphene clearly indicates binding between Ru and N. Differential charge density suggests charge redistribution, as shown in Figure 3b (right panel). In the inner regions of Ru cluster, a large area of electron loss is observed; these electrons are evidently captured by triNC. For nitrogen atoms, each gains about one more valence electron compared to original neutral nitrogen atom for Ru/triNC and Ru/NC by Bader charge analysis. Triazine-ring structure has a higher local nitrogen density; this correlates with the fact that the total electronic charge gathered by nitrogen in triNC is almost three times higher than that for NC. This result explains the observation of a much higher work function of triNC when compared to the work functions of NC and pure C. All these results confirm the electron transfer effect between Ru and support, and hence the contact electrification. It may be inferred that when supported on triNC, which has a much lower E_{Fermi}; Ru tends to lose more charge than in cases wherein Ru is loaded on NC or pure C. Thus, Ru behaves as a more 'positive surface' when loaded on triNC (Figure 3c). Considering the 'electron donor' surface that Ru becomes in the presence of triNC, on bonding with hydrogen; the degree of filling of bonding orbital (σ bond) would be reduced. This in turn would make the hydrogen adsorption weakens (Figure S11).[19]

2.3. Electrochemical HER performance

HER performance is measured in 1 M KOH solution using a three-electrode system at room temperature. The measurement requires the use of a surface-modified rotating disk electrode (RDE) as the working electrode and a graphite rod as a counter electrode. Three Ru catalysts with different carbon supports (Ru/C, Ru/NC, Ru/triNC) are tested. And Pt/triNC and commercial Pt/C (20 wt%, Johnson Matthey) are also tested for comparison. The HER performance is evaluated by the overpotential (η_{10}) versus reversible hydrogen electrode (RHE) at a current density of 10 mA cm^{-2}. As shown in Figure 4a, Ru/triNC shows excellent HER activity with a minimum overpotential of ~2 mV at a current density of 10 mA cm^{-2} (η_{10}: 2 mV). This is in fact much better than Ru/C (η_{10}: 80 mV) and Ru/NC (η_{10}: 43 mV). The observed HER activity of Ru/triNC represents a marked improvement when compared with a commercial Pt/C with a η_{10} of ~32 mV. These results indicate that Ru/triNC is the best-performing HER electrocatalyst in alkaline solution. By introducing N into C, Ru/NC shows an improvement and a Pt-like HER performance. This in fact quite unambiguously reflects the importance of N

doping in the carbon matrix. This is also consistent with the electron structure analysis mentioned above. The activity difference between Pt/C and Pt/triNC also demonstrates the importance and the specificity of the carbon support. In fact compared with commercial Pt/C, Pt/triNC reveals poorer activity with a large η_{10} of 67 mV, implying the negative role of the triazine-ring to decrease the HER activity of Pt. Moreover, commercial Ru/C (5wt%, Alfa Aesar) also shows a much lower HER activity with a large η_{10} of 87 mV when compared to Ru/triNC5 (Figure S12). This further demonstrates the key role of triazine-ring in boosting the HER activity of Ru. This is also consistent with the results presented above.

The kinetics of all these samples are investigated *via* Tafel plots (Figure 4b). Ru/triNC exhibits the lowest slope of Tafel plot of ~32.1 mV dec^{-1}, reflecting the occurrence of the Volmer-Tafel step on the surface of electrode; this would in fact be the fastest reaction (in terms of kinetics). For Pt/C, the slope of Tafel plot is higher (~41.3 mV dec^{-1}), demonstrating slower kinetics caused by the water dissociation step. However, replacing carbon by triNC for the Pt catalyst leads to a much higher slope of the Tafel plot of 111.2 mV dec^{-1}. This is possibly due to enhanced hydrogen adsorption, which in turn decreases the HER kinetics. Among Ru-based samples, N-free Ru/C has the highest slope associated with the Tafel plot (~105.5 mV dec^{-1}); this shows significantly slower kinetics caused by strong hydrogen adsorption onto the surface of Ru.

The differences between the HER performance of Ru/triNC and Pt/C in acidic and alkaline conditions are also analyzed (Figure S13). Ru/triNC exhibits excellent HER performance in alkaline conditions, while in acidic media it shows slow kinetics with a higher slope of Tafel plot (~39.8 mV dec^{-1}). On the other hand, Pt/C shows the opposite tendency. Pt/C performs better in an acidic electrolyte with a lower slope of Tafel plot (~25.0 mV dec^{-1}). This discrepancy might be caused by the spontaneous dissociation of water on Ru surface. In alkaline solution, the spontaneous dissociation of water on Ru surface provides abundant reactants (e.g., adsorbed H^+). But on Pt surface, a much higher overpotential is necessary to generate adsorbed proton. In acidic conditions, the strong interaction between Ru and the water molecule occupies active sites, lowering the HER kinetics. The moderate hydrogen adsorption and weak water interaction on Pt surface makes Pt a perfect HER catalyst in acidic conditions.[12]

Exchange current density of all samples is calculated using extrapolation of the Tafel plots (Figure 4b-c). Ru/triNC has an ultra-large exchange current density of 9.2 mA cm^{-2}, which is ~4 times higher than that of Pt/C (2.4 mA cm^{-2}). This implies an intrinsically high HER activity. It is also observed through electrochemical impedance spectroscopy (EIS) (Figure 4d). Ru/triNC shows the lowest charge transfer resistance. Electrochemical surface area (ECSA) is evaluated using CV scanning at different scan rates (Figure 4e, Figure S14 and Table S3). The capacitance of Ru/triNC is 89.9 mF cm^{-2}, revealing an extremely high ECSA. In fact, the ESCA value is found to be ~2 times higher than that of commercial Pt loaded onto carbon Vulcan XC72 (Pt/C). Pt/triNC also reveals a relatively high ECSA (101.7 mF cm^{-2}). This indicates the contribution of the carbon support (triNC) towards enhancing the ESCA. This result also confirms to the former reports of supercapacitors based on similar carbon materials.[24, 30] The durability measurements indicate that the η_{10} for Ru/triNC only increases by ~6 mV after 8000 cyclic voltammetry (CV) cycles (~8 h). In fact it once again shows that Ru/triNC significantly outperforms Pt/C (Figure 4f). Pt/C shows a large increase of η_{10} by ~12 mV in identical conditions.

Furthermore, the influence of synthesis parameters (Ru content: 1, 5, 10, 20 wt% and thermal treatment temperatures: 800, 900, 1000 °C) on Ru/triNC is investigated in detail. As shown in Figure 4g-i and Figure S15-16, Ru/triNC prepared at 900 °C shows the best HER activity. Other samples (Ru/triNC800 prepared at 800 °C and Ru/triNC1000 prepared at 1000 °C) reveal poorer activity than Ru/triNC. However they still perform much better than Pt/C. It is demonstrated that, as thermal treatment temperature increases, the content of triazine N decreases. This is due to the increased crystallization caused by the high-temperature

treatment. The N content in the carbon support, as well as the Ru loading amount is crucial to the final HER performance. Too much heteroatom doping is harmful to the conductivity of carbon support[31], while the lack of tri-N could influence the work function and further decrease the performance of loaded Ru nanoparticles. Therefore a moderate N content in the carbon support is necessary for obtaining the best HER performance. For the Ru loading amount, the high usage of Ru may cause the overgrowth of Ru nanoparticle in Ru/triNC20 (Figure S3d, e) and thus weaken the contact electrification between Ru and carbon support. Therefore it could lead to a poor HER performance. According to our experimental results,The optimized triazine N content is ca. 0.62 at% and the optimal Ru loading amount is 10 wt% (Figure 4h).

The mass activities of noble metals are also compared to that of Pt/C, Pt/triNC, and different Ru/triNC samples. These are related to the relative cost of hydrogen production (Figure 4i). The calculated mass activity of best Ru/triNC prepared at 900 °C (778.2 mA mg_{Ru}^{-1}) is >10 times higher than that of 20 wt% Pt/C (75.7 mA mg_{Pt}^{-1}) and >15 times higher than that of Pt/triNC (51.1 mA mg_{Pt}^{-1}) at 25 mV overpotential. Ru/triNC samples with different synthesis conditions also reveal mass activities which are better than that of Pt/C (193.3 mA mg_{Ru}^{-1} for Ru/triNC800, 381.5 mA mg_{Ru}^{-1} for Ru/triNC1000, 163.4 mA mg_{Ru}^{-1} for Ru/triNC1, 229.4 mA mg_{Ru}^{-1} for Ru/triNC5, 92.4 mA mg_{Ru}^{-1} for Ru/triNC20). Moreover, the turnover of frequency (TOF) of these samples is calculated and compared according to the metal loading amounts. The TOFs under the overpotential of 40 mV are 1.26 s^{-1} (per Ru atom) for Ru/triNC, 0.53 s^{-1} (per Pt atom) for Pt/C, 0.20 s^{-1} for Ru/NC and 0.07 s^{-1} for Ru/C, further illustrating the high HER activity of Ru/triNC. Also the optimized Ru/triNC is clearly shown to be superior to all Ru-based HER catalysts that have been reported over the last three years (Table S4).

2.4. DFT calculation for HER

Materials simulation based on density function theory (DFT) has been performed to gain further insights into electron transfer process between Ru and carbon supports and its effect on HER activity.[32] Calculation details are shown in the Methods section. For HER, generally, a moderate hydrogen adsorption Gibbs free energy ($\Delta G_H \approx 0$) is preferred to ensure fast hydrogen adsorption and desorption.[3, 4, 9, 33] The ΔG_H values for different catalysts and corresponding adsorption models are showed in Figure 5a and Figure S17. Compared to Pt, pure Ru surface exhibits a much higher ΔG_H (-0.02 eV for Pt(111) and -0.28 eV for Ru(001)). This is reasonably given in previous reports.[12] While loaded on carbon support, Ru exhibits weaker hydrogen binding than pure Ru (001). And the calculated ΔG_H values for Ru/C and Ru/NC are -0.20 eV and -0.17 eV, respectively. On the surface of Ru/triNC, hydrogen adsorption and desorption reveal an optimal thermodynamic process with a very small ΔG_H equal 0.04 eV. This value for Ru/triNC is significantly closer to ΔG_H on Pt surface. It is also close to the ideal value ($\Delta G_H \approx$ 0), indicating the superior HER activity of Ru/triNC. While for Pt/triNC, much stronger H adsorption (ΔG_H: -0.37 eV) is observed, which is due to the triNC carbon support. This leads to poor HER activity. These DFT calculations are therefore consistent with the experimental results we report.

As mentioned above, the ability of water dissociation on surface of catalyst is also an important indicator of HER especially in alkaline conditions. To simplify the calculation process, the ability of water dissociation is measured by calculating the H_2O binding energy (ΔE_w).[13, 17] Generally, a large ΔE_w is preferred for strong water molecule adsorption since it would weaken the O-H bond inside the water molecule and accelerate the dissociation process. The calculated ΔE_w values for different catalysts are shown in Figure 5b. As expected, Ru/triNC exhibits a much higher ΔE_w (0.41 eV) than Pt (0.11 eV for Pt(111)) and Ru (0.33 eV for Ru(001)), suggesting its significant ability for water dissociation. The difference between H_2O dissociation on surface of Pt, Ru, Ru/triNC, and Pt/triNC could also be observed in adsorption structure models after relaxation (Figure S18). On Pt surface, H_2O molecule is adsorbed resulting in the Pt-H bond, which is too weak to cleave O-H bond in H_2O. While on Ru surface,

H_2O molecule runs parallel to Ru(001) surface, demonstrating that the Ru-H bond and Ru-O bond have much larger binding energies. For Ru/triNC, the adsorption of H_2O mainly operates through the Ru-O bond. Although Ru-H bond is weakened, a larger ΔE_w is obtained. This reveals a much stronger Ru-O bond when H_2O molecule is adsorbed on Ru/triNC.[11] It may be attributed to electron loss resulting from increased contact electrification with the interface of Ru and triazine-ring. Ru with slight positive valence could in fact enhance the adsorption of oxygen-contained species. For Pt/triNC, interestingly, a much higher H_2O binding energy is observed, favoring water splitting. However, strong H adsorption leads to the slow kinetics of hydrogen evolution. Above all, the optimal hydrogen adsorption character and strong water dissociation ability makes Ru/triNC a champion HER catalyst in alkaline conditions.

3. Conclusion

We demonstrate that well-dispersed Ru nanoparticles on triazine-ring-doped carbon support (Ru/triNC) shows outstanding HER activity with an ultra-low overpotential of ~2 mV at 10 mA cm^{-2} and a small Tafel slope of ~32.1 mV dec^{-1} in alkaline electrolyte. The activity is significantly superior to that of (i) Pt/triNC made in the same way with the same metal concentration, and (ii) a commercial Pt/C catalyst. Also the observed activity is superior to any previously reported HER electrocatalysts.

The calculated mass activity of Ru/triNC (778.2 mA mg_{Ru}^{-1}) is over 10 times higher than that of commercial Pt/C (75.7 mA mg_{Pt}^{-1}) and over 15 times higher than that of Pt/triNC (51.1 mA mg_{Pt}^{-1}) at an overpotential of 25 mV. The key role of triazine ring doping in the triNC is confirmed by the XPS and UPS results, as well as DFT calculations. The doping of triazine ring into the carbon matrix changes the position of Fermi-level and the work function of the carbon support, making triNC a better electron acceptor compared with NC and pure C. The electron transfer from Ru to carbon support weakens the hydrogen adsorption intensity and accelerates the desorption of hydrogen during the HER. DFT calculation proves that a moderate hydrogen adsorption energy and stronge water dissociation ability are obtained on this contact electrification modified Ru surface, thus leading to a superior HER activity in alkaline medium. This finding offers insight into hydrogen evolution in alkaline solution and also suggests a feasible strategy to fabricate highly efficient Pt-free HER catalyst.

Supporting Information

Supporting Information is available from the Wiley Online Library or from the author.

Acknowledgements

The authors are grateful to the financial support from NSFC (51602332), the National Key Research and Development Program of China (2016YFB0700204), Science and Technology Commission of Shanghai Municipality (16DZ2260603, 19ZR1465100, 19ZR1479500), and Equipment Research Program (6140721050215). M. Yang would like to thank the National 1000 Youth Talents program of China and financial support from Ningbo 3315 program. T.T. thanks the Department of Science and Technology, and the Ministry of Electronics and Information Technology of the Govt. of India, for financial support. G.H. thanks the Chinese Academy of Science for PIFI funding.

References

[1] H. Yin, S. Zhao, K. Zhao, A. Muqsit, H. Tang, L. Chang, H. Zhao, Y. Gao, Z. Tang, Nature Communications 2015, 6, 6430; X. Cui, H.-Y. Su, R. Chen, L. Yu, J. Dong, C. Ma, S. Wang, J. Li, F. Yang, J. Xiao, M. Zhang, D. Ma, D. Deng, D. H. Zhang, Z. Tian, X. Bao, Nature Communications 2019, 10, 86.

[2] P. Li, M. Wang, X. Duan, L. Zheng, X. Cheng, Y. Zhang, Y. Kuang, Y. Li, Q. Ma, Z. Feng, W. Liu, X. Sun, Nature Communications 2019, 10, 1711.

[3] Z. W. Seh, J. Kibsgaard, C. F. Dickens, I. Chorkendorff, J. K. Nørskov, T. F. Jaramillo, Science 2017, 355, eaad4998.

[4] I. A. Pašti, E. Fako, A. S. Dobrota, N. López, N. V. Skorodumova, S. V. Mentus, ACS Catalysis 2019, 9, 3467.

[5] E. Skúlason, G. S. Karlberg, J. Rossmeisl, T. Bligaard, J. Greeley, H. Jónsson, J. K. Nørskov, Physical Chemistry Chemical Physics 2007, 9, 3241.

[6] D. Strmcnik, P. P. Lopes, B. Genorio, V. R. Stamenkovic, N. M. Markovic, Nano Energy 2016, 29, 29.

[7] Y. Zheng, Y. Jiao, A. Vasileff, S.-Z. Qiao, Angewandte Chemie International Edition 2018, 57, 7568.

[8] N. Danilovic, R. Subbaraman, D. Strmcnik, K.-C. Chang, A. P. Paulikas, V. R. Stamenkovic, N. M. Markovic, Angewandte Chemie International Edition 2012, 51, 12495; R. Subbaraman, D. Tripkovic, D. Strmcnik, K.-C. Chang, M. Uchimura, A. P. Paulikas, V. Stamenkovic, N. M. Markovic, Science 2011, 334, 1256.

[9] C.-T. Dinh, A. Jain, F. P. G. de Arquer, P. De Luna, J. Li, N. Wang, X. Zheng, J. Cai, B. Z. Gregory, O. Voznyy, B. Zhang, M. Liu, D. Sinton, E. J. Crumlin, E. H. Sargent, Nature Energy 2019, 4, 107.

[10] L. Birry, A. Lasia, Journal of Applied Electrochemistry 2004, 34, 735; P. Los, A. Rami, A. Lasia, Journal of Applied Electrochemistry 1993, 23, 135.

[11] A. Shavorskiy, M. J. Gladys, G. Held, Physical Chemistry Chemical Physics 2008, 10, 6150; J. Weissenrieder, A. Mikkelsen, J. N. Andersen, P. J. Feibelman, G. Held, Physical Review Letters 2004, 93, 196102.

[12] Y. Zheng, Y. Jiao, Y. Zhu, L. H. Li, Y. Han, Y. Chen, M. Jaroniec, S.-Z. Qiao, Journal of the American Chemical Society 2016, 138, 16174.

[13] J. Mao, C.-T. He, J. Pei, W. Chen, D. He, Y. He, Z. Zhuang, C. Chen, Q. Peng, D. Wang, Y. Li, Nature Communications 2018, 9, 4958.

[14] W. Li, Y. Liu, M. Wu, X. Feng, S. A. T. Redfern, Y. Shang, X. Yong, T. Feng, K. Wu, Z. Liu, B. Li, Z. Chen, J. S. Tse, S. Lu, B. Yang, Advanced Materials 2018, 30, 1800676.

[15] Y. Li, L. A. Zhang, Y. Qin, F. Chu, Y. Kong, Y. Tao, Y. Li, Y. Bu, D. Ding, M. Liu, ACS Catalysis 2018, 8, 5714.

[16] J. Mahmood, F. Li, S.-M. Jung, M. S. Okyay, I. Ahmad, S.-J. Kim, N. Park, H. Y. Jeong, J.-B. Baek, Nature Nanotechnology 2017, 12, 441.

[17] Q. Song, X. Qiao, L. Liu, Z. Xue, C. Huang, T. Wang, Chemical Communications 2019, 55, 965.

[18] J. Xu, T. Liu, J. Li, B. Li, Y. Liu, B. Zhang, D. Xiong, I. Amorim, W. Li, L. Liu, Energy & Environmental Science 2018, 11, 1819; Z.-L. Wang, K. Sun, J. Henzie, X. Hao, C. Li, T. Takei, Y.-M. Kang, Y. Yamauchi, Angewandte Chemie International Edition 2018, 57, 5848; J. Zhang, P. Liu, G. Wang, P. P. Zhang, X. D. Zhuang, M. W. Chen, I. M. Weidinger, X. L. Feng, Journal of Materials Chemistry A 2017, 5, 25314.

[19] T. Ling, T. Zhang, B. Ge, L. Han, L. Zheng, F. Lin, Z. Xu, W.-B. Hu, X.-W. Du, K. Davey, S.-Z. Qiao, Advanced Materials 2019, 31, 1807771.

[20] P. Feulner, D. Menzel, Surface Science 1985, 154, 465.

[21] L. Tao, Y. Wang, Y. Zou, N. Zhang, Y. Zhang, Y. Wu, Y. Wang, R. Chen, S. Wang, Advanced Energy Materials 2019, 0, 1901227.
[22] R. G. Horn, D. T. Smith, Science 1992, 256, 362.
[23] Z. Zhuang, Y. Li, Z. Li, F. Lv, Z. Lang, K. Zhao, L. Zhou, L. Moskaleva, S. Guo, L. Mai, Angewandte Chemie International Edition 2018, 57, 496.
[24] Y. Li, S. Zheng, X. Liu, P. Li, L. Sun, R. Yang, S. Wang, Z.-S. Wu, X. Bao, W.-Q. Deng, Angewandte Chemie International Edition 2018, 57, 7992.
[25] P. Kuhn, M. Antonietti, A. Thomas, Angewandte Chemie International Edition 2008, 47, 3450; S.-Y. Yu, J. Mahmood, H.-J. Noh, J.-M. Seo, S.-M. Jung, S.-H. Shin, Y.-K. Im, I.-Y. Jeon, J.-B. Baek, Angewandte Chemie International Edition 2018, 57, 8438.
[26] Y. Li, F. Chu, Y. Liu, Y. Kong, Y. Tao, Y. Li, Y. Qin, Chemical Communications 2018, 54, 13076; U. Joshi, S. Malkhandi, Y. Ren, T. L. Tan, S. Y. Chiam, B. S. Yeo, ACS Applied Materials & Interfaces 2018, 10, 6354; J. Wang, Z. Wei, S. Mao, H. Li, Y. Wang, Energy & Environmental Science 2018, 11, 800.
[27] M. Wissler, Journal of Power Sources 2006, 156, 142.
[28] Y. Shi, K. K. Kim, A. Reina, M. Hofmann, L.-J. Li, J. Kong, ACS Nano 2010, 4, 2689.
[29] E. R. Kötz, H. Neff, K. Müller, Journal of Electroanalytical Chemistry and Interfacial Electrochemistry 1986, 215, 331.
[30] L. Hao, B. Luo, X. Li, M. Jin, Y. Fang, Z. Tang, Y. Jia, M. Liang, A. Thomas, J. Yang, L. Zhi, Energy & Environmental Science 2012, 5, 9747; L. Hao, J. Ning, B. Luo, B. Wang, Y. Zhang, Z. Tang, J. Yang, A. Thomas, L. Zhi, Journal of the American Chemical Society 2015, 137, 219.
[31] K. Fujisawa, T. Tojo, H. Muramatsu, A. L. Elías, S. M. Vega-Díaz, F. Tristán-López, J. H. Kim, T. Hayashi, Y. A. Kim, M. Endo, M. Terrones, Nanoscale 2011, 3, 4359; Z. R. Ismagilov, A. E. Shalagina, O. Y. Podyacheva, A. V. Ischenko, L. S. Kibis, A. I. Boronin, Y. A. Chesalov, D. I. Kochubey, A. I. Romanenko, O. B. Anikeeva, T. I. Buryakov, E. N. Tkachev, Carbon 2009, 47, 1922.
[32] F. Aguilera-Granja, L. C. Balbás, A. Vega, The Journal of Physical Chemistry A 2009, 113, 13483; H.-Y. T. Chen, S. Tosoni, G. Pacchioni, The Journal of Physical Chemistry C 2015, 119, 10856.
[33] H. Chen, X. Ai, W. Liu, Z. Xie, W. Feng, W. Chen, X. Zou, Angewandte Chemie International Edition 2019, 58, 11409.

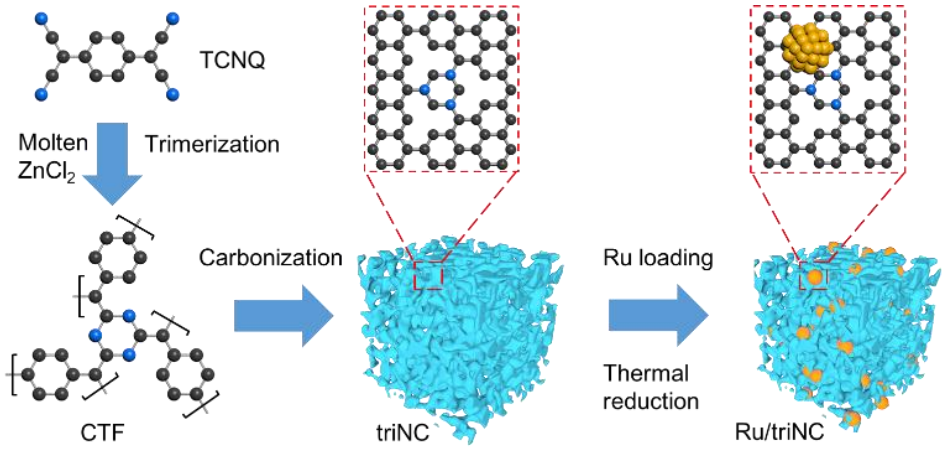

Scheme 1. Schematic illustration of synthesis of Ru/triNC. Black, blue and orange spheres represent C, N and Ru atoms, respectively.

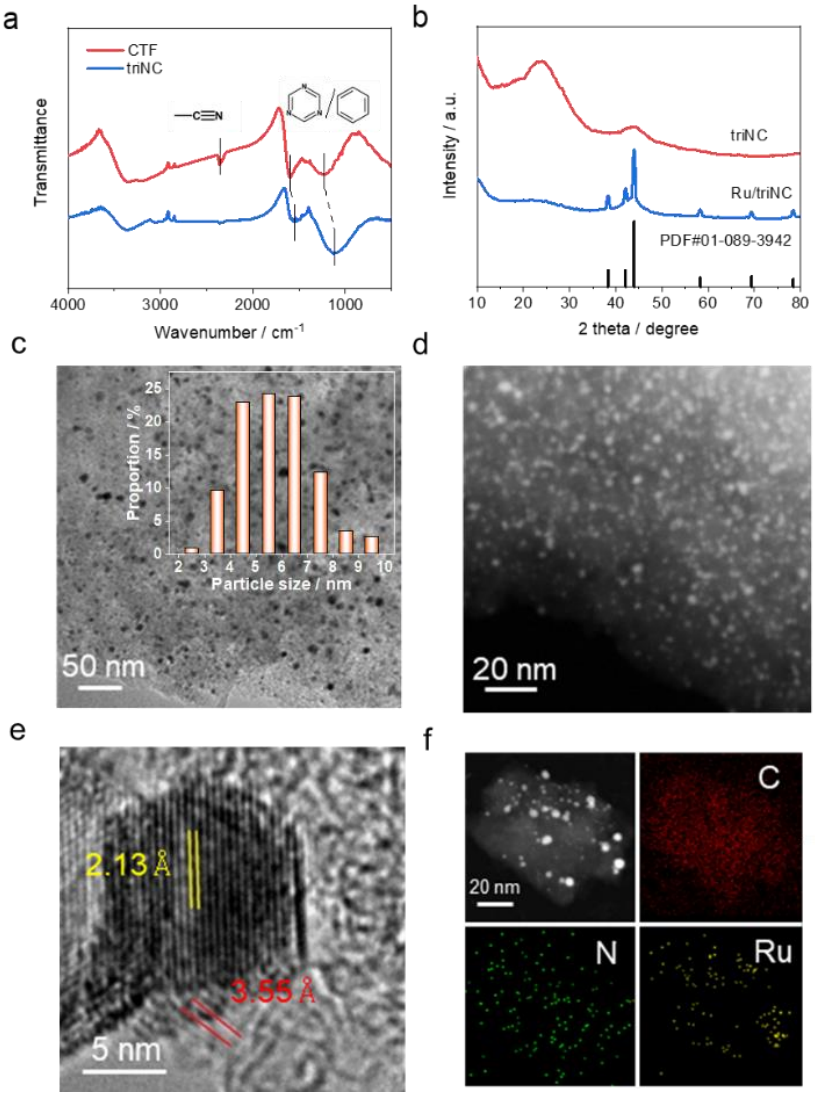

Figure 1. (a) FT-IR spectra of triazine-based CTF and triNC. (b) XRD patterns of triNC and Ru/triNC. (c-d) TEM and HADDF-STEM images of Ru/triNC. Inset of (c) is particle size distribution of Ru nanoparticles. (e) HRTEM image of Ru/triNC. (f) HAADF-STEM images of Ru/triNC and the corresponding elemental mapping images for C, N and Ru.

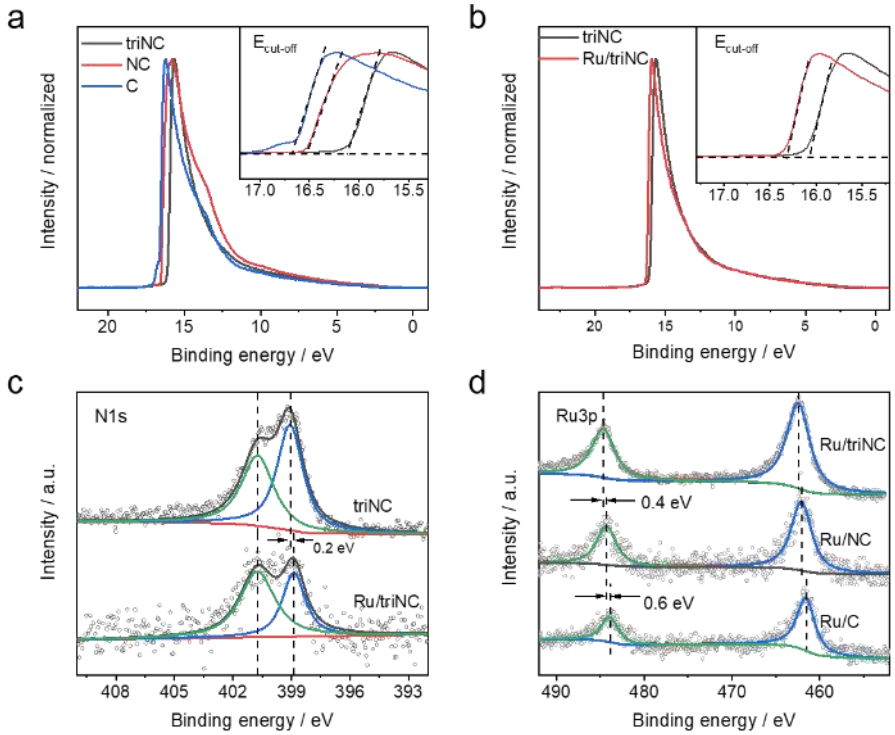

Figure 2. Electronic properties of carbon supports and Ru-loaded samples. UPS spectra of (a) C, NC, and triNC, and (b) Ru/triNC and triNC. The insets show the enlarged parts. XPS spectra of (c) N1s of triNC and Ru/triNC, and (d) Ru3p of Ru/C, Ru/NC, and Ru/triNC.

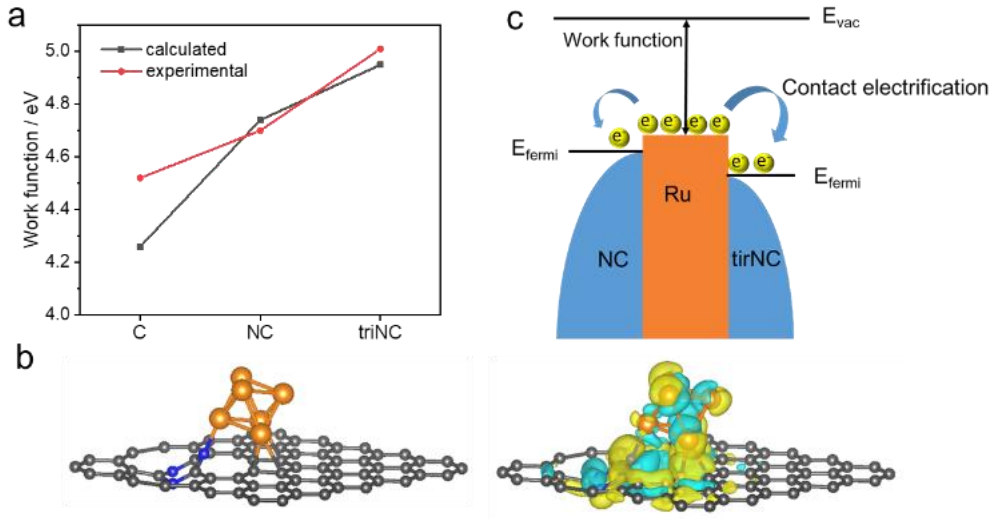

Figure 3. (a) Experimental and calculated work functions of C, NC and triNC support. (b) Differential charge density of Ru/triNC. Grey, blue and orange spheres represent C, N and Ru atoms, respectively. Yellow and blue areas represent electron accumulation and electron depletion, respectively. (c) Illustration of contact electrification in Ru/triNC and Ru/NC, showing increased contact electrification in Ru/triNC.

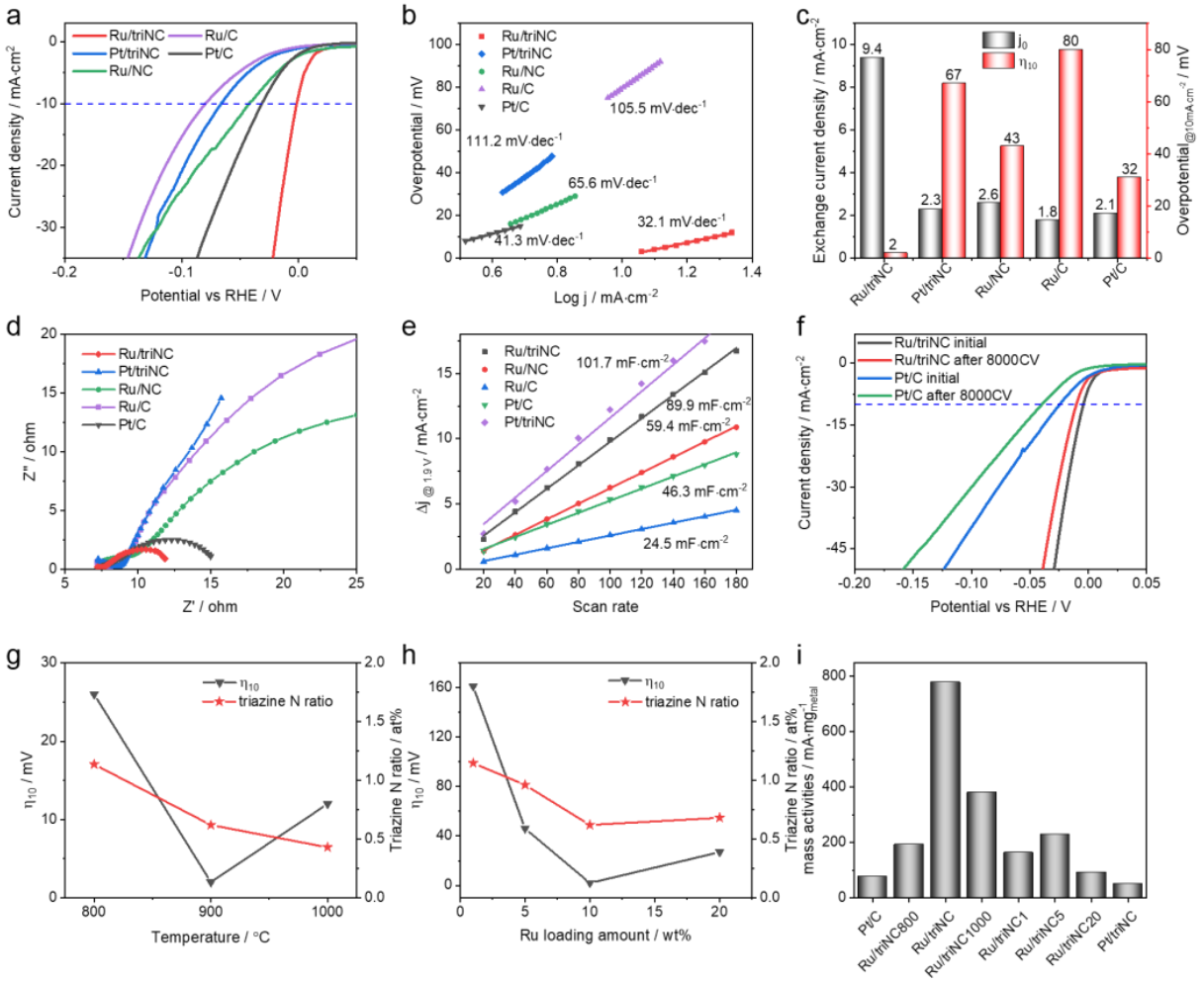

Figure 4. (a) LSV curves for Ru/triNC, Ru/NC, Ru/C and commercial Pt/C in 1 KOH solution (scan rate: 2 mV s^{-1}; rotation speed: 1600 rpm; iR correction: 90%). (b) Tafel plots calculated from the data in a. (c) Comparison of overpotential at a current density of 10 mA cm^{-2} and exchange current density calculated using extrapolation of Tafel plots. (d) EIS spectra. (e) Electrochemical surface area measured by double layer capacitance. (f) Duration measurements of commercial Pt/C and Ru/triNC. (g and h) Dependence of η_{10} and triazine N content for Ru/triNC on thermal treatment temperatures and Ru loading amounts. (i) Comparison of metal mass activities (at 25 mV overpotential) for Pt/C, Pt/triNC, and Ru/triNC with different thermal treatment temperatures and Ru loading amounts.

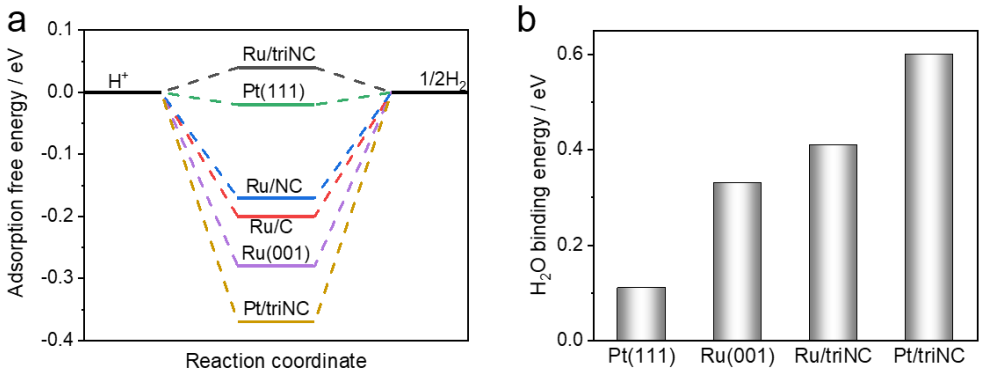

Figure 5. (a) Hydrogen adsorption free energy (ΔG_H) on Ru/triNC, Pt/triNC, Ru/C, Ru/NC, Pt (111) and Ru (001). (b) Water molecule binding energy on Pt(111), Ru(001), Ru/triNC, and Pt/triNC.

Triazine-ring as an active “electron acceptor” is a good match for ruthenium to weaken the hydrogen binding on ruthenium through interfacial charge transfer *via* increased contact electrification confimed by both theoretical and experimental results. The resulting ruthenium triazine composites exhibits the outstanding HER activity when compared to commercial Pt/C in alkaline solution.

Keyword: electrocatalysis, nanocomposite, electron acceptor, contact electrification, theoretical calculation

Qiangjian Ju, Ruguang Ma,* Yu Pei, Beibei Guo, Zichuang Li, Qian Liu, Tiju Thomas, Minghui Yang,* Graham J. Hutchings, and Jiacheng Wang*

Ruthenium Triazine Composite: A Good Match for Increasing Hydrogen Evolution Activity through Contact Electrification